Gated-STED Microscopy with Sub-Nanosecond Pulsed Fiber Laser for Reducing Photobleaching

Marco Castello[1,4], Giorgio Tortarolo[1,4], Iván Coto Hernández[2,#], Paolo Bianchini[2], Mauro Buttafava[3], Gianluca Boso[3,§], Alberto Tosi[3], Alberto Diaspro[2,5,6] and Giuseppe Vicidomini[1,]*

[1]Molecular Microscopy and Spectroscopy, Nanophysics, Istituto Italiano di Tecnologia, Via Morego 30, 16163, Genoa, Italy; [2]Nanoscopy, Istituto Italiano di Tecnologia, Via Morego 30, 16163, Genoa, Italy; [3]Dipartimento di Elettronica, Informazione e Bioingegneria, Politecnico di Milano, Piazza Leonardo da Vinci, 32, 20133, Milan, Italy; [4]Department of Informatics, Bioengineering, Robotics and Systems Engineering, University of Genoa, Via Opera Pia 13, 16145, Genoa, Italy; [5]Department of Physics, University of Genoa, Via Dodecaneso 33, 16146, Genoa, Italy; [6]Nikon Imaging Center, Istituto Italiano di Tecnologia, Via Morego 30, 16163 Genoa, Italy.

[*]Correspondence to: Giuseppe Vicidomini, Molecular Microscopy and Spectroscopy, Nanophysics, Istituto Italiano di Tecnologia. E-mail: giuseppe.vicidomini@iit.it

[#]Current address: Institut des Sciences Moléculaires d'Orsay, CNRS, Université Paris Sud, Université Paris-Saclay, F91405, Orsay Cedex, France

[§]Current address: Group of Applied Physics, University of Geneva, Chemin de

Pinchat 22, CH-1211, Genève 4, Switzerland

Keywords: super-resolved microscopy, time-gated detection, non-linear photobleaching, STED microscopy

ABSTRACT

The spatial resolution of a stimulated emission depletion (STED) microscope is theoretically unlimited and practically determined by the signal-to-noise ratio. Typically, an increase of the STED beam's power leads to an improvement of the effective resolution. However, this improvement may vanish because an increased STED beam's power is often accompanied by an increased photobleaching, which worsen the effective resolution by reducing the signal strength.

A way to lower the photobleaching in pulsed STED (P-STED) implementations is to reduce the peak intensity lengthening the pulses duration (for a given average STED beam's power). This also leads to a reduction of the fluorophores quenching, thus a reduction of the effective resolution, but the time-gated detection was proved to be successful in recovering these reductions.

Here we demonstrated that a sub-nanosecond fiber laser beam (pulse width ~ 600 ps) reduces the photobleaching with respect to a traditional stretched hundreds picosecond (~ 200 ps) beam provided by a Ti:Sapphire laser, without any effective spatial resolution lost.

INTRODUCTION

In stimulated emission depletion (STED) microscopy, the process of stimulated emission transiently quenches (switch-off) fluorophores at predefined positions of the diffraction-limited excited regions of a conventional microscope. As a consequence only the fluorescent signal stemming from fluorophores located in the complementary regions, which can reach sub-diffraction sized, is registered. Scanning these regions across the sample allows to build up images with sub-diffraction spatial resolution. In the single point STED implementation the excited region is a conventional Gaussian focal spot and the stimulated emission is a doughnut-shaped focal spot featuring a "zero"-intensity point in the center. By co-aligning the excitation beam and the stimulated emission beam, the so-called STED beam, the fluorescence is confined in a tiny sub-diffraction sized region around the "zero"-intensity point.

Theoretically, the spatial resolution of a STED microscope is unlimited (Hell and Wichmann, 1994). Namely, all sample's frequencies are transmitted by the STED microscope (Hell and others, 2015). However, practically the resolution is determined by the signal to noise ratio (SNR): the highest frequency of the sample that emerges from the noise determines the effective resolution. The most used and reliable way to improve the effective resolution in a STED microscope is increasing the intensity of the STED beam, which shrinks the effective fluorescent region and directly leads to an absolute enhancement of the strength of the sample's high frequencies. However, the increase in intensity of the STED beam is normally accompanied by an increase in photobleaching, thus by a reduction of the SNR and potentially of the effective resolution. In essence, photobleaching limits the effective resolution of STED microscopy.

It has been shown that a prominent cause of photobleaching in STED microscopy

experiments is the population of higher-order excited-states (singlet or triplet) due to the absorption of stimulating photons (belonging to the STED beam) from an excited-state (singlet or triplet) (Donnert and others, 2009; Donnert and others, 2006; Hotta and others, 2010). Here, the fluorophore most likely reacts with the environment and the photobleaching takes place. The reduction of the population of these higher-order excited-states is at the base of most of the strategies to reduce photobleaching in STED microscopy, such as: (i) the choice of a STED beam wavelength outside the region from which the fluorophore can absorb (in particular absorption from any excited-states) (Hotta and others, 2010; Rankin and others, 2011); (ii) a fast beam scanning implementation (Schneider and others, 2015; Wu and others, 2015b) or a large pulse-to-pulse interval (Donnert and others, 2009; Donnert and others, 2006), which allows the fluorophore to relax from the triplet state before the arrival of the successive STED beam pulse; (iii) the intramolecular photo-stabilization of synthetic organic fluorophores *via* triplet state quenching (van der Velde and others, 2016). Notably, because of the long duration (> μs) of the triplet (excited-state), a fluorophore in this state has a high cumulative probability to absorb a stimulating photon.

A different approach, not strictly linked to the depopulation of the higher-order excited-states, pre-drives the fluorescent probes subject to high doses of stimulating photons into a state where the probes are ”inert” both to excitation and stimulated emission (Danzl and others, 2016). However, this approach lacks in generality, since it requires fluorescent probes with an “inert” state (thus, different from the triplet state), such as photo-switchable proteins.

A less explored approach is the reduction of the peak intensity (for a fix average intensity) of the STED beam by lengthening the pulse-width (Dyba and Hell, 2003).

Indeed, the multi-steps nature of the fluorophore transitions to the higher-order excited-states(Eggeling and others, 1998) leads to a non-linear dependency of the photobleaching with the STED beam (peak) intensity. Thus, the use of long pulses, such as the one provided by (sub-)nanosecond (> 500 ps) pulsed laser (Bianchini and others, 2015; Bottanelli and others, 2016; Gottfert and others, 2013), can reduce the photobleaching, with respect to shorter pulses. On the other side, for a given STED beam's average intensity, the longer is the pulse the lower is the fluorophore quenching and thus the effective resolution (Leutenegger and others, 2010; Moffitt and others, 2011; Vicidomini and others, 2013). In essence, if the pulse-width of the STED beam is comparable with the excited-state lifetime of the fluorophores, the stimulating photons acting on the fluorophores when they are in the excited-state are typically fewer, and a non-negligible part of the fluorophores still emits fluorescence (because they were not exposed to enough stimulating photons) (Moffitt and others, 2011; Vicidomini and others, 2013). In the typical doughnut-based STED implementation, such unwanted fluorescence signal is particularly relevant outside the centre of the doughnut, where the STED beam intensity is lower, thus the effective fluorescence confinement is reduced and the resolution degraded.

For these reasons, a trade-off between photobleaching and effective resolution must be reached when choosing the pulse-width of the STED beam. Early STED implementations obtained such a compromise with 100-200 ps pulse-width (Gould and others, 2011; Vicidomini and others, 2015a; Wu and others, 2015a).

The introduction of time-gated detection can relax the conditions for meeting this compromise. In particular, it allows using long pulse-width for photobleaching reduction without degradation of the resolution. Indeed, by collecting the fluorescence immediately after the action of the STED pulses, the depletion efficiency (i.e. the

ability to silence a fluorophore) does not depend on the pulse-width (thus on the peak intensity), but on the average intensity(Moffitt and others, 2011; Vicidomini and others, 2013). Notably, time-gated detection does not enhance the fluorescence quenching, but the depletion efficiency. Namely, a reduction of the absolute fluorescence signal can be obtained only by increasing the intensity of the STED beam. However, collecting the fluorescence only after the whole duration of the STED beam ensures that the fluorophore from which the signal is collected has resided (statistically) in the excited state for all the duration of the STED beam's pulse and thus has been subject to all the stimulating photons. As a result, whilst the absolute depletion (fluorescence quenching) does not change with the time-gated detection the effective depletion (signal silencing) improves.

Here we show that the use of a ~600 ps pulse-width STED beam provided by a fiber laser reduces the photobleaching in a STED imaging experiment with respect of using the ~200 ps pulse-width STED beam typically provided by a Ti:Sapphire laser (properly stretched). Whilst, the spatial resolution reduction associated to the relative long pulse-width is fully compensated by time-gating the fluorescence signal.

MATERIALS AND METHODS

STED Microscope

We built a custom-made pulsed STED (P-STED) microscope as depicted in Figure 1. The excitation beam was provided by a triggerable pulsed diode laser (LDH-D-C-640, Picoquant) emitting at 640 nm. The STED beam was provided by a femtosecond (~ 160 fs) mode-locked Ti:Sapphire laser (Chameleon Ultra II Coherent) running at 775 nm or by a sub-nanosecond (~ 580 ps) fiber laser (Katana HP, Onefive GmbH) emitting at 775 nm. We coupled both laser beams (one at a time) into the very same

100 m long polarization maintaining fiber (PMF), which transfers the beams to the microscope. The use of the same PMF allows maintaining the STED and excitation beams co-alignment when switching between the two STED beams. Indeed, the end of the PMF fiber is never unplugged from the "microscope body".

Before injection into the PMF, the Ti:Sapphire laser beam passed through two 20 cm long glass rods (GRs) to temporally stretch the pulse-width to few picosecond in order to avoid unwanted non-linear effects and damages during the fiber coupling. Then we injected the beam into the PMF to further temporally spread the pulses up to ~ 170 ps. Due to the narrow spectra width (> 0.1nm) and the long pulse width (~ 580 ps) of the fiber laser, the injection of its beam into the PMF does not introduce significant temporal pulse stretch. For each incoming beam we used a half-wave plate (HWP) to adjust its polarization parallel to the fast axis of the PMF. We controlled the power of the STED beam through a laser power control (LPC) or through the laser driver, for the Ti:Sapphire laser and the fiber laser beams, respectively. We controlled the power of the excitation beam through an acoustic optical modulator (AOM, MT110-A1-IR, AAopto-electronic). Both the Ti:Sapphire laser and the fiber laser (master) run at 80 MHz and provide an electronic reference signal which we used to synchronize electronically the excitation laser diode (slave). We used a picosecond electronic delayer (Picosecond Delayer, Micro Photon Devices) to temporal align the excitation and STED beam. The STED beam emerging from the PMF is collimated, filtered in polarization by a rotating Glan–Thompson polarizing prism (GTP) and phase-engineered though a polymeric mask imprinting 0–2π helical phase-ramps (VPP-1a, RPC Photonics). We rotated a quarter-wave plate (QWP) and a half-wave-plate (HWP) to obtain circular polarization of the STED beam at the back-aperture of the objective lens. We co-aligned the excitation and STED beam using two dichroic

mirrors (T750SPXRXT and H643LPXR, AHF Analysentechnik). The beams were deflected by two galvanometric scanning mirrors (6215HM40B, CTI-Cambridge) and directed toward the objective lens (CFI Plan Apo VC 60x Oil, Nikon) by the same set of scan and tube lenses used in a commercial scanning microscope (Confocal C2, Nikon). The fluorescence light was collected by the same objective lens, de-scanned, and passed through the dichroic mirrors as well as through a fluorescence band pass filter (685-70, AHF analysentechnik) before being focused (focal length 60 mm, Thorlabs) into a multi-mode fiber (MMF) and acquired by an avalanche photo diode (APD) (SPCM-AQRH-13-FC, PerkinElmer).

We implemented the time-gated detection with an upgraded version of the high-throughput gated photon counter (gated box) developed by Boso et al (Boso and others, 2014). The new version handles repetition rate up to 100 MHz, gate width from 70 ps to 10 ns and provides a TTL output for each gated photon (within the time-gate). The gated output and the un-gated output (directly from the APD) were delivered to an FPGA-based data-acquisition card (NI USB-7856R from National Instruments), which is controlled by the custom-written software Carma. The software-package Carma controls the entire microscope devices needed during the image acquisition, such as the galvanometric mirrors and the AOM, and visualizes the data.

Synchronization of the gated-detection with the excitation events is obtained through the reference signal provided by the excitation laser diode. Notably, the excitation laser diode acts as slave of the lasers (one at a time) providing the STED beam. Another picosecond electronic delayer (Picosecond Delayer, Micro Photon Devices) allowed locating the time-gated detection at different delay with respect to the excitation events, for example immediately after the excitation events ($T_g = 0$ ns) or

after the STED beam action ($T_g = T_{STED}$). In order to find the reference position $t = 0$ ns located immediately after the excitation events, we changed the position of the time-gate until we reached the maximization of the fluorescence signal for a confocal imaging experiment (no STED beam active). Notably, the reference position will be different for the two STED beam configurations, since the associated laser (the fiber laser or the Ti:Sapphire laser) acts, one at a time, as master.

RESULTS

It has been shown that, for a given average power, the larger is the pulse-width of the STED beam the lower is the photobleaching (Dyba and Hell, 2003), but also the lower is the fluorescent quenching (Leutenegger and others, 2010; Moffitt and others, 2011; Vicidomini and others, 2013), hence, the poorer is the effective resolution. Thus, in a STED imaging experiment, the reduction of the photobleaching comes at the cost of the reduction of the spatial resolution. Fortunately, the reduction in resolution due to large pulse-width can be fully recovered by using time-gated detection (Moffitt and others, 2011; Vicidomini and others, 2011; Vicidomini and others, 2013).

We first demonstrated that, for a given average power of the STED beam (P_{STED} = 39 mW, measured at the back-aperture of the objective lens), the two lasers generate significantly different images. Figure 2 compares side-by-side the confocal, the conventional P-STED and the gated P-STED (gP-STED) images for calibration fluorescent beads (60 nm sized crimson beads, Invitrogen) in the two laser configurations, the ~200 ps pulse-width (Fig. 2 a-c) and the ~600 ps pulse-width (Fig. 2 d-f), respectively. Very important, since both lasers run at the same wavelength and emerge from the same PMF, no spatial alignment is required when switching from

one laser to the other. By reflection imaging of sub-diffraction gold beads we verified that the doughnut-shaped intensity distributions at the focus for the two laser beams are identical. On the other side, when switching between the two lasers, it was necessary to temporal align the excitation and the STED beam. In both configurations, we straightforwardly aligned the excitation and STED beams using a picosecond electronic delayer: for a given laser and a given average STED beam power ($P_{STED} > 0$ mW), we changed the delay until we reached the maximum fluorescence quenching. Notably, the temporal alignments have been performed removing the phase-mask, that produces the doughnut-shaped focus, thus using the STED beams in a Gaussian configuration. Because the relatively short pulse-width ($T_{STED} \sim 200$ ps *versus* an excited-state lifetime of $\tau_{S1} \sim 3.7$ ns) provided by the Ti.Sapphire laser (opportunely stretched), the fluorescence emitted during the action of the STED beam is negligible and the time-gated detection does not offer any benefit (Fig. 2 b,c). On the contrary, for longer pulse-width ($T_{STED} \sim 600$ ps) the fluorescence during the STED beam action is not anymore negligible and the STED image shows a reduction of contrast and thus effective resolution. However, the contrast is fully recovered if the early fluorescence ($0<t<T_g$, with $T_g = T_{STED}$) is discarded, i.e. if a time-gated detection is applied (Fig. 2 e,f). We collected the conventional and the gated P-STED simultaneously by splitting the signal from the APD in two identical signals. The first is filtered in time (gP-STED) whilst the second reached the acquisition card unaffected (P-STED).

The benefits of time-gated detection when using relatively long pulse-width for the STED beam are also highlighted in case of microtubules imaging. Figure 3 compares side-by-side the confocal, the conventional P-STED and the gated P-STED (gP-STED) images for beta-tubulin ATTO647N labeled COS 7 cells. Because even in this

case the pulse-width of the fiber laser is not negligible with respect to the excited-state lifetime of the fluorophore (T_{STED} ~ 200 ps *versus* an excited-state lifetime of τ_{S1} ~ 4 ns) , the enhancement of the effective resolution, obtained by rejecting the early photons immediately after the excitation events ($0 < t < T_g$, with $T_g = T_{STED}$) is consitent (Fig. 3 b,c). Notably, (i) we used a relatively low power for the STED beam, as a consequence the P-STED images show small improvements with respect to the confocal counterparts; (ii) to obtain similar resolution with the P-STED modality it would be necessary to increase the intensity of the STED beam, which however may introduce substantial photobleaching and cancel-out the expected resolution enhancement.

In this context, it is important to remember that also the reduction of signal associated to the time-gating may cancel-out the expected resolution enhancement. However, the signal reduction reported in our experiments does not translate in substantial image degradation. These results have been achieved also thanks to the implementation of the time-gated detection with a gated-box (instead of a time-correlated-single-photon-counting (TCSPC) card). Indeed, because the gated-box does not introduce any substantial dead-time, it allows to fully explore the maximum count-rate of the detector without any signal loss typical of the TCSPC card (Coto Hernàndez and others, 2015).

However, for other imaging conditions, such as fast imaging and/or low fluorescent photon-flux, time-gated detection may substantially reduce the SNR. In this case the SNR can be recovered through dedicated multi-image deconvolution algorithms, which re-integrate the early-photons usually discarded into the restored image (Castello and others, 2014; Coto Hernández and others, 2016). Another imaging condition in which time-gated detection may engrave the image quality is when the

STED beam directly generates a fluorescence background, the so-called anti-Stokes emission background (Vicidomini and others, 2012). In all our experiments, we set the power of the excitation beam (P_{exc} = 3 μW, measured at the back-aperture of the objective lens) such that -Stokes emission background is negligible with respect to the desired fluorescence signal. Above all, different synchronous detection methods has been proposed to compensate for situation in which the anti-Stokes emission background is not negligible and increasing the power of the excitation beam is not a viable solution (Coto Hernández and others, 2016; Coto Hernàndez and others, 2014; Ronzitti and others, 2013; Vicidomini and others, 2012).

Successively we demonstrated that, for a given average power (P_{STED} = 39 mW, measured at the back-aperture of the objective lens), the ~ 600 ps STED pulses provided by a fiber laser reduces the photobleaching with respect to the ~ 200 ps STED pulses provided by a Ti:Sapphire laser (opportunely stretched). Within this scope, we collected a series of STED images of beta-tubulin ATTO647N labeled COS 7 cells, using the two different lasers.

Figure 4 shows the STED image brightness as a function of the frame number normalized to the first frame (in each series) for the two laser beam implementations. No time-gated detection is performed on the images. As expected, the photobleaching reduces for longer pulse-width of the STED beam. Importantly, this reduction of photo bleaching is fully compatible with all the other methods, such as the fast beam scanning implementation and the photo-stabilization of synthetic organic fluorophores *via* triple-state quenching.

DISCUSSION

Different experimental conditions have been used to reduce photobleaching in STED experiments. These approaches are based on low repetition-rate lasers, fast scanning

implementation, triplet state quenching or photoswitchable proteins. A less explored approach, compatible with the all methods proposed above, is the lengthening of the STED pulses. Albeit the relation between STED pulse-width and photobleaching is well known, the reduction of fluorescence quenching for increasing STED pulse-width has precluded, in the past, the use of (sub-)nanosecond pulse lasers. The recent introduction of time-gated detection in the STED microscope compensated for such a reduction, thus opening the use of (sub-)nanosecond/nanoseconds lasers for efficient STED implementations. Here we showed that combining a sub-nanosecond fiber laser as STED and a time-gated box it is possible to obtain an effective STED implementation with reduced photobleaching.

It is worth-noting that in a time-gated STED system the fluorescent signal stemming from the center of the detection volume reduces as a function of the time-delay T_g. Namely, the signal reduces exponentially as $\exp(-T_g/\tau_{S1})$, with τ_{S1} the excited-state lifetime of the unperturbed (no stimulated emission) fluorophore. Because in a gated pulsed STED implementation the time-delay T_g coincides with the STED beam's pulse-width $T_{STED} = 600$ ps and the excited-state lifetime τ_{S1} of the most used fluorophores is > 2.9 ns, the signal reduces less than 20%. This signal reduction leads to a 10% reduction of the SNR, thus to a potential reduction of the effective-resolution. Even if in our experiments the 10% SNR reduction does not reflect in visible resolution degradation, it may be possible that in other imaging conditions the SNR improvement obtained by the reduction of photobleaching does not compensate the SNR reduction introduced by the time-gated detection. However, also in these worse cases the combination of long pulse-width beam and time-gated leads to some benefits. First, in case of live-cell imaging, photobleaching is usually accompanied by phototoxicity, thus photobleaching reduction can be important independently by the

potentially associated resolution improvement. Furthermore, the reduction of the photobleaching is essential to records consecutive images of the sample (Schneider and others, 2015), which is typical for cellular dynamic studies, and when the STED microscopy concept is combined with fluorescence correlation spectroscopy (FCS) (Eggeling and others, 2009; Vicidomini and others, 2015b). Last but not least, the SNR reduction induced by time-gated detection can be recovered by using multi-image deconvolution algorithms (Castello and others, 2014; Coto Hernández and others, 2016).

In addition to the relative long pulse-width that reduces the photobleaching, the sub-nanosecond fiber laser used in this report has two other features important in the contest of STED microscopy: (i) the capability to be externally triggered and (ii) the narrow spectra width. The possibility to trigger the laser avoids complex and expensive optical synchronization and temporal alignment between the excitation and STED beam, thus greatly simplifies the STED microscopy architectures. For example, the near-infrared fiber laser used in this work opens for a powerful and straightforward implementation of two-photon excitation (2PE) STED (2PE-STED) microscopy in the near-infrared spectral region. The current pulsed 2PE-STED implementations (Bethge and others, 2013; Li and others, 2009; Takasaki and others, 2013) require two synchronized Ti:Sapphire lasers which provide respectively the STED and the 2PE beams. Replacing the Ti:Sapphire used as STED beam with the triggerable fiber laser greatly reduces costs and complexity.

The narrow spectra width of the fiber laser (~1 nm versus ~15 nm of the stretched Ti:Sapphire laser) perfectly harmonizes with the phase plate used to generate the doughnut. Indeed, beams with broad spectrum width fills up quickly the “zero”-intensity of the doughnut, inducing fluorescence quenching also at the “zero”-

intensity point and thus reducing the effective resolution of the STED microscope (Galiani and others, 2012). Furthermore, the narrow spectrum allows also for a more efficient suppression of the scattered light which potential reaches the detector.

ACKNOWLEDGEMENTS

We thank Michele Oneto (Nanoscopy, Istituto Italiano di Tecnologia) for assistance with the sample preparation and immunolabeling, the Onefive GmbH for laser supporting and Nikon Corporation for technical supporting.

REFERENCES

Bethge P, Chereau R, Avignone E, Marsicano G, Nagerl UV. 2013. Two-photon excitation STED microscopy in two colors in acute brain slices. Biophys J 104(4): 778-785.

Bianchini P, Peres C, Oneto M, Galiani S, Vicidomini G, Diaspro A. 2015. STED nanoscopy: a glimpse into the future. Cell Tissue Res 360(1): 143-50.

Boso G, Tosi A, Mora AD, Zappa F. 2014. High-throughput gated photon counter with two detection windows programmable down to 70 ps width. Rev Sci Instrum 85(1): 013107.

Bottanelli F, Kromann EB, Allgeyer ES, Erdmann RS, Wood Baguley S, Sirinakis G, Schepartz A, Baddeley D, Toomre DK, Rothman JE, Bewersdorf J. 2016. Two-colour live-cell nanoscale imaging of intracellular targets. Nat Commun 7.

Castello M, Diaspro A, Vicidomini G. 2014. Multi-images deconvolution improves signal-to-noise ratio on gated stimulated emission depletion microscopy. Appl Phys Lett 105(23): 234106.

Coto Hernàndez I, Buttafava M, Boso G, Diaspro A, Tosi A, Vicidomini G. 2015. Gated STED microscopy with time-gated single-photon avalanche diode. Biomed Opt Express 6(6): 2258-2267.

Coto Hernández I, Castello M, Lanzanò L, d'Amora M, Bianchini P, Diaspro A, Vicidomini G. 2016. Two-Photon Excitation STED Microscopy with Time-Gated Detection. Sci. Rep. 6: 19419-19419 EP.

Coto Hernàndez I, Peres C, Cella Zanacchi F, d'Amora M, Christodoulou S, Bianchini P, Diaspro A, Vicidomini G. 2014. A new filtering technique for removing

anti-Stokes emission background in gated CW-STED microscopy. J Biophotonics 7(6): 376-380.

Danzl JG, Sidenstein SC, Gregor C, Urban NT, Ilgen P, Jakobs S, Hell SW. 2016. Coordinate-targeted fluorescence nanoscopy with multiple off states. Nat Photon 10(2): 122-128.

Donnert G, Eggeling C, Hell SW. 2009. Triplet-relaxation microscopy with bunched pulsed excitation. Photochem. Photobiol. Sci. 8: 481-485.

Donnert G, Keller J, Medda R, Andrei MA, Rizzoli SO, Lührmann R, Jahn R, Eggeling C, Hell SW. 2006. Macromolecular-scale resolution in biological fluorescence microscopy. Proceedings of the National Academy of Sciences 103(31): 11440-11445.

Dyba M, Hell SW. 2003. Photostability of a Fluorescent Marker Under Pulsed Excited-State Depletion through Stimulated Emission. Appl Opt 42(25): 5123-5129.

Eggeling C, Ringemann C, Medda R, Schwarzmann G, Sandhoff K, Polyakova S, Belov VN, Hein B, von Middendorff C, Schonle A, Hell SW. 2009. Direct observation of the nanoscale dynamics of membrane lipids in a living cell. Nature 457(7233): 1159-1162.

Eggeling C, Widengren J, Rigler R, Seidel CAM. 1998. Photobleaching of Fluorescent Dyes under Conditions Used for Single-Molecule Detection: Evidence of Two-Step Photolysis. Anal Chem 70(13): 2651-2659.

Galiani S, Harke B, Vicidomini G, Lignani G, Benfenati F, Diaspro A, Bianchini P. 2012. Strategies to maximize the performance of a STED microscope. Opt Express 20(7): 7362-7374.

Gottfert F, Wurm CA, Mueller V, Berning S, Cordes VC, Honigmann A, Hell SW. 2013. Coaligned Dual-Channel STED Nanoscopy and Molecular Diffusion Analysis at 20 nm Resolution. Biophys J 105(1): L01-L03.

Gould TJ, Myers JR, Bewersdorf J. 2011. Total internal reflection STED microscopy. Opt Express 19(14): 13351-13357.

Hell SW, Sahl SJ, Bates M, Zhuang X, Heintzmann R, Booth MJ, Bewersdorf J, Shtengel G, Hess H, Tinnefeld P, Honigmann A, Jakobs S, Testa I, Cognet L, Lounis B, Ewers H, Davis SJ, Eggeling C, Klenerman D, Willig KI, Vicidomini G, Castello M, Diaspro A, Cordes T. 2015. The 2015 super-resolution microscopy roadmap. J. Phys. D: Appl. Phys 48(44): 443001-443001.

Hell SW, Wichmann J. 1994. Breaking the diffraction resolution limit by stimulated emission: stimulated-emission-depletion fluorescence microscopy. Opt. Lett. 19(11): 780-782.

Hotta J-i, Fron E, Dedecker P, Janssen KPF, Li C, Müllen K, Harke B, Bückers J, Hell SW, Hofkens J. 2010. Spectroscopic Rationale for Efficient Stimulated-Emission Depletion Microscopy Fluorophores. J Am Chem Soc 132(14): 5021-5023.

Leutenegger M, Eggeling C, Hell SW. 2010. Analytical description of STED microscopy performance. Opt Express 18(25): 26417-26429.

Li Q, Wu SSH, Chou KC. 2009. Subdiffraction-limit two-photon fluorescence microscopy for GFP-tagged cell imaging. Biophys J 97(12): 3224-3228.

Moffitt JR, Osseforth C, Michaelis J. 2011. Time-gating improves the spatial resolution of STED microscopy. Opt Express 19(5): 4242-4254.

Rankin BR, Moneron G, Wurm CA, Nelson JC, Walter A, Schwarzer D, Schroeder J, Colón-Ramos DA, Hell SW. 2011. Nanoscopy in a Living Multicellular Organism Expressing GFP. Biophys J 100(12): L63-L65.

Ronzitti E, Harke B, Diaspro A. 2013. Frequency dependent detection in a STED microscope using modulated excitation light. Opt Express 21(1): 210-219.

Schneider J, Zahn J, Maglione M, Sigrist SJ, Marquard J, Chojnacki J, Krausslich H-G, Sahl SJ, Engelhardt J, Hell SW. 2015. Ultrafast, temporally stochastic STED nanoscopy of millisecond dynamics. Nat Meth 12(9): 827-830.

Takasaki KT, Ding JB, Sabatini BL. 2013. Live-Cell Superresolution Imaging by Pulsed STED Two-Photon Excitation Microscopy. Biophys J 104(4): 770-777.

van der Velde JHM, Oelerich J, Huang J, Smit JH, Aminian Jazi A, Galiani S, Kolmakov K, Guoridis G, Eggeling C, Herrmann A, Roelfes G, Cordes T. 2016. A simple and versatile design concept for fluorophore derivatives with intramolecular photostabilization. Nat Commun 7.

Vicidomini G, Coto Hernàndez I, Diaspro A, Galiani S, Eggeling C. 2015a. The Importance of Photon Arrival Times in STED Microscopy. In: Advanced Photon Counting. Kapusta P, Wahl M, Erdmann R, editors: Springer International Publishing. pp 283-301.

Vicidomini G, Haisen T, Mueller V, Honigmann A, Clausen MP, Waithe D, Sezgin E, Diaspro A, Hell SW, Eggeling C. 2015b. Spatio-temporal heterogeneity of lipid membrane dynamics revealed by STED-FLCS. Nano Lett 15(9): 5912–5918.

Vicidomini G, Moneron G, Eggeling C, Rittweger E, Hell SW. 2012. STED with wavelengths closer to the emission maximum. Opt Express 20(5): 5225-5236.

Vicidomini G, Moneron G, Han KY, Westphal V, Ta H, Reuss M, Engelhardt J, Eggeling C, Hell SW. 2011. Sharper low-power STED nanoscopy by time gating. Nat Methods 8(7): 571-573.

Vicidomini G, Schönle A, Ta H, Han KY, Moneron G, Eggeling C, Hell SW. 2013. STED Nanoscopy with Time-Gated Detection: Theoretical and Experimental Aspects. PLoS ONE 8(1): e54421.

Wu X, Toro L, Stefani E, Wu Y. 2015a. Ultrafast photon counting applied to resonant scanning STED microscopy. J Microsc 257(1): 31-38.

Wu Y, Wu X, Lu R, Zhang J, Toro L, Stefani E. 2015b. Resonant Scanning with Large Field of View Reduces Photobleaching and Enhances Fluorescence Yield in STED Microscopy. Sci. Rep. 5: 14766-14766 EP.

Figure 1. Experimental setup for (g)P-STED microscopy. AOM: Acousto-optic modulator; GTP: Glan–Thompson polarizer; PM: phase mask; HWP: half-wave plate; QWP: quarter-wave plate; DM: dichroic mirror; GMs: galvometer mirrors; SL: scanning lens; TL: tube lens; OL: objective lens; 3AS: three-axis stage; BPF: band-pass filter; AD: achromatic doublet; PMF: polarized maintaining fiber; MF: multi-mode fiber; APD: avalanche photo-diode; FPGA: field programmable gate-array; FI: Faraday isolator; LPC: laser-power control; GR: glass rod; BE: beam expander.

Figure 2. Imaging comparison between hundreds picosecond and sub-nanosecond STED beams. Confocal (a,d), P-STED (b,e) and gated P-STED (c,f) imaging of calibration 60 nm fluorescent beads (P_{STED} = 39 mW, $T_g = T_{STED}$). Images clearly reveal the different effects of time-gated detection for STED microscopy when using hundreds picoseconds (T_{STED} ~ 200 ps) STED beam (b,c) or sub-nanoseconds (T_{STED} ~ 600 ps) STED beam (e,f). Whilst time-gated detection does not produce any contrast or resolution enhancement when using the hundreds picoseconds STED beam, the enhancement is evident when using the sub-nanoseconds STED beam. Notably, in the case of sub-nanoseconds STED beam the time-gated detection allows to recover the decrease in contrast induced by the relative longer pulse-width. Indeed, because the average power in the two laser configurations is the same, a resolution enhancement with respect to the hundreds picoseconds STED beam it is not expected. Insets show magnified views of the marked areas. Scale bars 1 μm.

Figure 3. Comparison of confocal, P-STED and gated P-STED imaging with sub-nanosecond STED beam. Imaging of beta-tubulin ATTO647 N labeled cell (a-c, P_{STED} = 39 mW). Images clearly reveal the importance of applying time-gated detection when using relative long pulse-width for the STED beam. Insets show magnified views of the marked areas, renormalized in signal intensity. Scale bars 1 μm.

Figure 4. Reduced photobleaching using sub-nanosecond STED beam. Image brightness (not gated) as a function of frame number normalized to the first frame in each series for hundreds picoseconds (~ 200 ps) STED beam (red circles) and sub-nanoseconds (~ 600 ps) STED beam (black squares). The very same imaging configurations and parameters have been used for both laser beams (P_{STED} = 45 mW). Mean ± standard deviation of measurements in five different beta-tubulin ATTO 647N labeled cells.

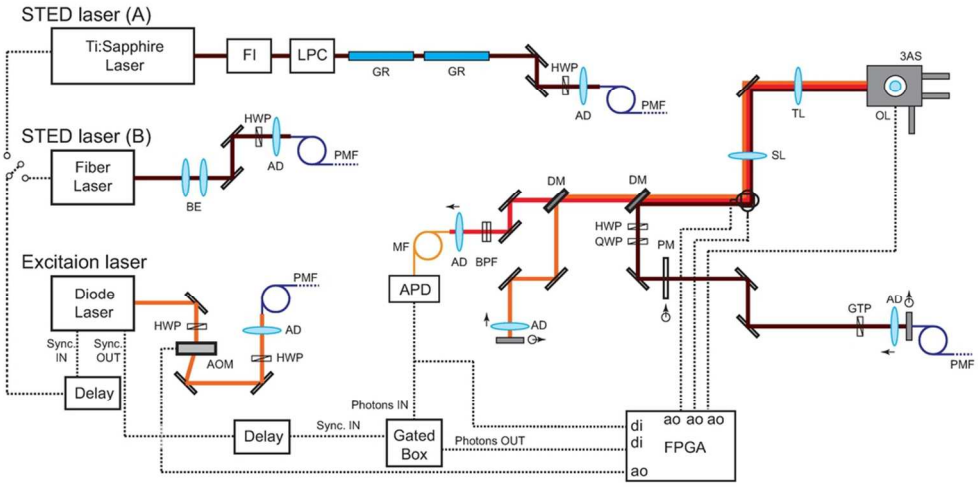

94x48mm (300 x 300 DPI)

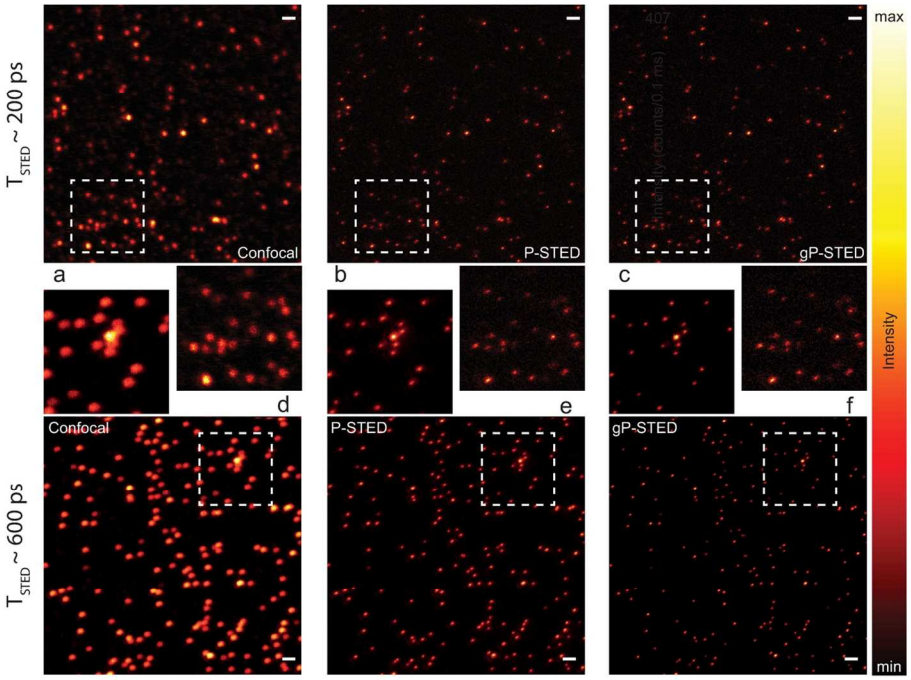

127x88mm (300 x 300 DPI)

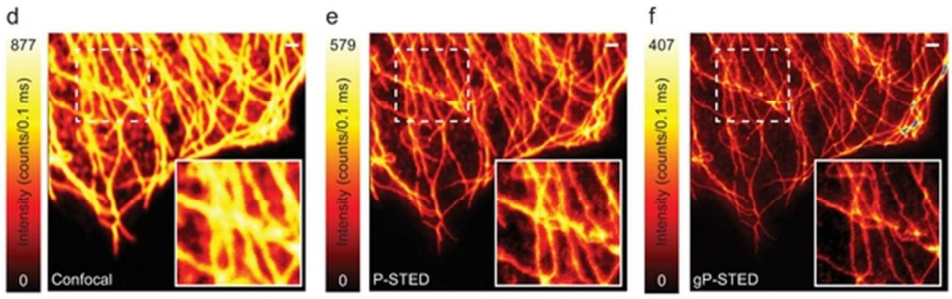

53x15mm (300 x 300 DPI)

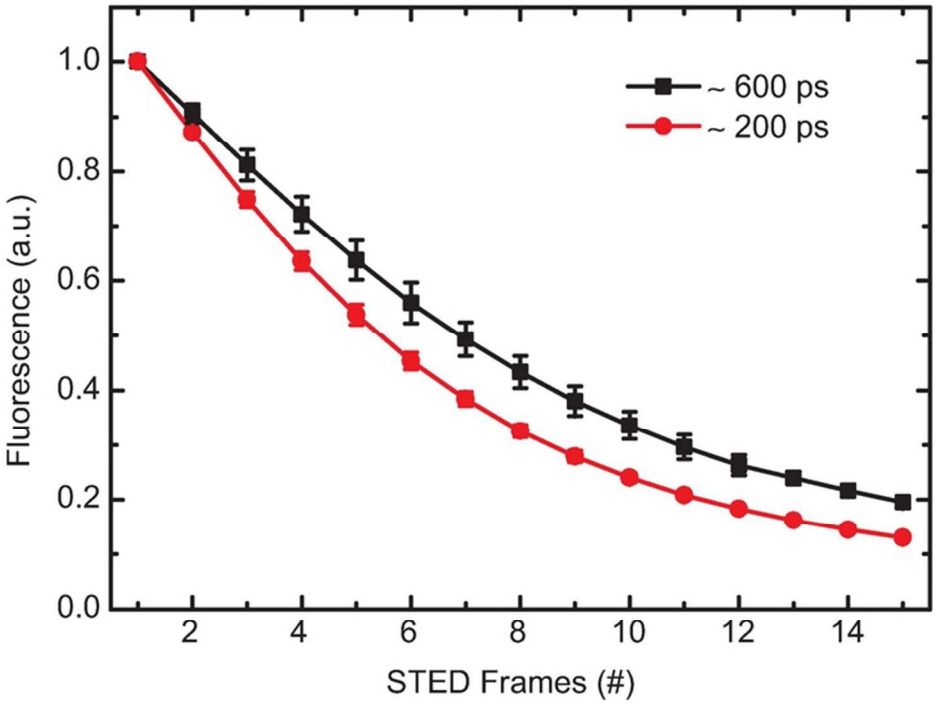

67x51mm (300 x 300 DPI)